DOI: 10.1021/ic900931r

Inorganic Chemistry
Article

Combination Chemistry of Hexa-Copper-Substituted Polyoxometalates Driven by the Cu^{II}−Polyhedra Distortion: From Tetramer, 1D Chain to 3D Framework

Bing Li,[†,§] Jun-Wei Zhao,[†] Shou-Tian Zheng,[†] and Guo-Yu Yang*[,†,‡]

[†]*State Key Laboratory of Structural Chemistry, Fujian Institute of Research on the Structure of Matter, Chinese Academy of Sciences, Fuzhou, Fujian 350002, China,* [‡]*Department of Chemistry, Beijing Institute of Technology, Beijing 100081, China, and* [§]*Department of Chemistry, Zhejiang Forestry University, Lin'an, Zhejiang 311300, China*

Received May 12, 2009

Reaction of $CuCl_2 \cdot 2H_2O$ and trivacant Keggin polyoxoanion $Na_9[A\text{-}\alpha\text{-}PW_9O_{34}] \cdot 7H_2O$ in the presence of ethylenediamine/1,2-diaminopropane (en/enMe) under hydrothermal conditions led to five novel inorganic−organic hybrid polyoxotungstates (POTs):$[Cu(en)_2]_2[Cu(en)_2(H_2O)]_2[Cu(H_2O)_2][Cu_4(H_2O)_2(B\text{-}\alpha\text{-}PW_9O_{34})_2] \cdot 2H_2O$(**1**), $[Cu_6(\mu_3\text{−}OH)_3(en)_3(H_2O)_5(B\text{-}\alpha\text{-}PW_9O_{34})] \cdot 6H_2O$ (**2**), $Na_6\{[Cu_6(\mu_3\text{−}OH)_3(en)_3(H_2O)_2(B\text{-}\alpha\text{-}PW_9O_{34})]_2[Cu_4(H_2O)_2(B\text{-}\alpha\text{-}PW_9O_{34})_2]\} \cdot 2\ H_2en \cdot 8H_2O$ (**3**), $[Cu_6(\mu_3\text{−}OH)_3(en)_3(H_2O)_3(B\text{-}\alpha\text{-}PW_9O_{34})] \cdot 4H_2O$ (**4**), $[Cu^{II}{}_6Cu^{I}{}_4(\mu_6\text{-}O)(OH)_{18}][Cu_6(\mu_3\text{−}OH)_3(enMe)_3(H_2O)_3(B\text{-}\alpha\text{-}PW_9O_{34})]_4 \cdot 4H_3O \cdot 2H_2O$ (**5**). **1** is a new 1D chain constructed from alternate tetra-Cu^{II} sandwiched units $[Cu^{II}{}_4(H_2O)_2(B\text{-}\alpha\text{-}PW_9O_{34})_2]^{10-}$ and dinuclear $[Cu^{II}{}_2(H_2O)_6]^{4+}$ units. **2**−**5** are a series of novel transition-metal substituted polyoxometalates (TMSPs) comprising hexa-Cu^{II} substituted {**Cu_6PW_9**} units (**Cu_6**=$Cu_6(\mu_3\text{−}OH)_3$, **PW_9**=B-α-PW_9O_{34}, Scheme 1). **2** is an unusual monomer. **3** is an unprecedented tetramer built by two types of TMSP units, [**Cu_6PW_9**$(en)_3(H_2O)_2$] and $[Cu^{II}{}_4(H_2O)_2$(**PW_9**$)_2]^{10-}$. **4** is a novel chain assembled from [**Cu_6PW_9**$(en)_3(H_2O)_3$] units by double-bridging mode. Most interestingly, **5** is a open framework made by [**Cu_6PW_9**$(enMe)_3(H_2O)_3$] units, in which the novel decacopper oxygen clusters, $[Cu^{I}{}_4Cu^{II}{}_6(\mu_6\text{-}O)(OH)_{18}]^{4-}$ formed in situ, are encapsulated into the channels, and **5** represents the first decametallic-cluster-containing open framework built by TMSP units. **2**−**5** all contain the hexa-Cu^{II} substituted POT unit {**$Cu_6PW_9L_3(H_2O)_n$**} (L = en/enMe, $n < 6$) made by {**$Cu_6L_3(H_2O)_n$**} core and trivacant Keggin **PW_9** fragments. Moreover, **3**−**5** can be viewed as combining derivatives of **2** through substituting water ligands on hexa-Cu^{II} {**$Cu_6L_3(H_2O)_n$**} units by terminal oxygen atoms of **PW_9** units. Importantly, the Cu^{II}-polyhedra Jahn−Tell/pseudo-Jahn−Teller distortion plays a crucial role in the formation of **1**−**5**. The magnetic behaviors of **2**−**5** show antiferromagnetic interactions between the Cu^{II} ions in the hexa-Cu^{II} cluster.

Introduction

The rational self-assembly of modular and multicomponent systems into larger structures or materials with useful properties remains an intense focus of current research.[1] However, the problem faced by chemists is the selection of systems that can be synthesized or self-assembled in a predetermined manner to form highly complicated architectures without reorganizing other unknown fragments. In this aspect, it is interesting to examine the functional polyoxotungstates (POTs) as ideal inorganic building blocks to construct the aforementioned functionally solids.[2]

Lacunary Keggin-type POTs are can be easily prepared in one- or two-step processes in high yields and act as the stable reactive precursors in solution in variable concentrations and temperature.[3] Reaction of stable, lacunary POT fragments with transition-metal (TM) ions usually leads to products with unchanged lacunary Keggin-type POTs.[2] Depending upon the coordination requirement and the size of a given TM ion, the geometry of the reaction product can therefore often be predicted. In the past several decades, many novel TM-substituted polyoxometalates (TMSPs) have been made by incorporating TM cations into the skeleton of POT

*To whom correspondence should be addressed. E-mail: ygy@fjirsm.ac.cn. Fax: 86 591-8371-0051.

(1) (a) Leclerc-Laronze, N.; Haouas, M.; Marrot, J; Taulelle, F.; Hervé, G. *Angew. Chem., Int. Ed.* **2006**, *45*, 139. (b) Mller, A.; Peters, F.; Pope, M. T.; Gatteschi, D. *Chem. Rev.* **1998**, *98*, 239. (c) Cronin, L.; Beugholt, C.; Krickemeyer, E.; Schmidtmann, M.; Bögge, H.; Kögerler, P.; Luong, T. K. K.; Mller, A. *Angew. Chem., Int. Ed.* **2002**, *41*, 2805.

(2) (a) Mialane, P.; Dolbecq, A.; Marrot, J.; Rivière, E.; Sécheresse, F. *Angew. Chem., Int. Ed.* **2003**, *42*, 3523. (b) Mal, S. S.; Kortz, U. *Angew. Chem., Int. Ed.* **2005**, *44*, 3777. (c) Clemente-Juan, J. M.; Coronado, E.; Galán-Mascarós, J. R.; Gómez-García, C. J. *Inorg. Chem.* **1999**, *38*, 55. (d) Mialane, P.; Dolbecq, A.; Marrot, J.; Rivière, E.; Sécheresse, F. *Chem.—Eur. J.* **2005**, *11*, 1771. (e) Bassil, B. S.; Nellutla, S.; Kortz, U.; Stowe, A. C.; Van Tol, J.; Dalal, N. S.; Keita, B.; Nadjo, L. *Inorg. Chem.* **2005**, *44*, 2659. (f) Godin, B.; Chen, Y.; Vaissermann, J.; Ruhlmann, L.; Verdaguer, M.; Gouzerh, P. *Angew. Chem., Int. Ed.* **2005**, *44*, 3072. (g) Pichon, C.; Mialane, P.; Dolbecq, A.; Marrot, J.; Rivière, E.; Bassil, B. S.; Kortz, U.; Keita, B.; Nadjo, L.; Sécheresse, F. *Inorg. Chem.* **2008**, *47*, 11120.

(3) Ginsberg, A. P. *Inorg. Synth.* **1990**, *27*, 100.

Published on Web 07/27/2009

fragments by means of conventional aqueous solution methods.[2] However, the rational tailoring and assembly of in situ formed TMSP units remains a great challenge.

Recently, we are focusing on the investigation on the reactivity of lacunary POTs and TM cations under hydrothermal conditions and have successfully isolated a series of novel TMSPs[4−7] including hexa-TM-substituted monomers, $[Ni(L)_2]_m[Ni_6(\mu_3{-}OH)_3(L)_{3n}(H_2O)_{6-2n}(B\text{-}\alpha\text{-}XW_9O_{34})]\cdot yH_2O$ (L = organoamines, X = $P^V/Si^{IV}/Ge^{IV}$) and $[Cu_6(\mu_3{-}OH)_3(en)_3(H_2O)_3(B\text{-}\alpha\text{-}PW_9O_{34})]\cdot 7H_2O$,[4] and tetra-/hexa-/octa-TM sandwiched dimers.[4−7] The water ligands on hexa-TM units of in situ formed TMSP monomers can be substituted by terminal oxygen atoms of POTs[4a,4c,7] or carboxylic oxygen atoms,[4a,4b] resulting in novel open-frameworks constituted by same type of TMSP structural building units (SBUs).[4a−4c,7] Therefore, it is possible that the larger aggregates or extended frameworks can be assembled by different types of TMSP SBUs formed in situ under rational conditions. We chose the Cu^{II} ion to react with lacunary POTs for making larger aggregates or extended frameworks built by Cu-substituted SBUs based on the following considerations: (1) The Cu^{II} ion shows more flexible coordination geometries (trigonal bipyramid, square pyramid and octahedron) than the Ni^{II} ion (octahedron); (2) especially, because of the coexistence of octahedral and square pyramidal geometries of the Cu^{II} ions, the Jahn−Teller effect of the octahedra, pseudo-Jahn−Teller effect of the square pyramids, and different linkage modes may overcome larger steric hindrance and help to stabilize the in situ formed larger aggregates, leading to novel isomers or configurations. Thus, a family of novel hybrid organic−inorganic octa-Cu sandwiched POTs $H_4[Cu^{II}_8(dap)_4(H_2O)_2(B\text{-}\alpha\text{-}GeW_9O_{34})_2]\cdot 13H_2O$, $(H_2en)_2[Cu^{II}_8(en)_4(H_2O)_2(B\text{-}\alpha\text{-}GeW_9O_{34})_2]\cdot 5H_2O$, $(H_2en)_2[Cu^{II}_8(en)_4(H_2O)_2(B\text{-}\alpha\text{-}SiW_9O_{34})_2]\cdot 8H_2O$, $[Cu^{II}(H_2O)_2]H_2[Cu^{II}_8(en)_4(H_2O)_2(B\text{-}\alpha\text{-}XW_9O_{34})_2]$ (X = Si^{IV}/Ge^{IV}) and $[Cu^{II}_2(H_2O)_2(2,2'\text{-bpy})_2]\{[Cu^{II}(bdyl)]_2[Cu_8(2,2'\text{-bpy})_4(H_2O)_2(B\text{-}\alpha\text{-}GeW_9O_{34})_2]\}\cdot 4H_2O$ (bdyl = 2,2'-bipyridinyl) have been successfully made.[7] In addition, a $6^5\cdot 8$ $CdSO_4$-type 3D framework built by hexa-Cu^{II} sandwiched POTs $[Cu(en)_2]_2[Cu(deta)(H_2O)]_2[Cu_6(en)_2(H_2O)_2(B\text{-}\alpha\text{-}GeW_9O_{34})_2]\cdot 6H_2O$ has been synthesized by us.[6b] As an extension of our work, we again successfully obtained a series of novel hybrid inorganic−organic TMSPs: $[Cu(en)_2]_2[Cu(en)_2(H_2O)]_2[Cu(H_2O)_2][Cu_4(H_2O)_2(B\text{-}\alpha\text{-}PW_9O_{34})_2]\cdot 2H_2O$(**1**), $[Cu_6(\mu_3{-}OH)_3(en)_3(H_2O)_5(B\text{-}\alpha\text{-}PW_9O_{34})]\cdot 6H_2O$(**2**), $Na_6\{[Cu_6(\mu_3{-}OH)_3(en)_3(H_2O)_2(B\text{-}\alpha\text{-}PW_9O_{34})]_2[Cu_4(H_2O)_2(B\text{-}\alpha\text{-}PW_9O_{34})_2]\}\cdot 2H_2en\cdot 8H_2O$ (**3**), $[Cu_6(\mu_3{-}OH)_3(en)_3(H_2O)_3(B\text{-}\alpha\text{-}PW_9O_{34})]\cdot 4H_2O$ (**4**), $[Cu^{II}_6Cu^{I}_4(\mu_6\text{-}O)(OH)_{18}][Cu_6(\mu_3{-}OH)_3(enMe)_3(H_2O)_3(B\text{-}\alpha\text{-}PW_9O_{34})]_4\cdot 4H_3O\cdot 2H_2O$ (**5**) (en/enMe = ethylenediamine/1,2-diaminopropane).

Scheme 1. Structures of (a) the Cu_6 Core, (b) the PW_9 Fragment, and (c) the $\{Cu_6PW_9\}$ SBU Assembled by the Cu_6 Core and the PW_9 Fragments

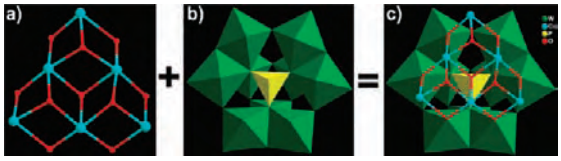

Experimental Section

Materials and Methods. The starting material $Na_9[A\text{-}\alpha\text{-}PW_9O_{34}]\cdot 7H_2O$ (A-α-PW_9) was prepared as in the literature method.[3] All other chemicals are reagent grade and used as purchased without further purification. Elemental analyses (C, H, and N) were performed by using a PE 2400 II elemental analyzer. IR spectra were obtained by means of an ABB Bomen MB 102 spectrometer with pressed KBr pellets in the range of 4000−400 cm^{-1}. Thermogravimetric analyses (TGA) were performed by using a Mettler TGA/SDTA851 thermal analyzer in the temperature region of 30−800 °C under a dry air atmosphere for **2**−**4** and under a dry nitrogen atmosphere for **5** with the heating rate of 10 °C/min. Magnetic susceptibility measurements were carried out using a Quantum Design MPMS-5 magnetometer in the temperature range of 2−300 K. The susceptibility data were corrected from the diamagnetic contributions as deduced by using PascalRs constant tables.

$[Cu(en)_2]_2[Cu(en)_2(H_2O)]_2[Cu(H_2O)_2][Cu_4(H_2O)_2(B\text{-}\alpha\text{-}PW_9O_{34})_2]\cdot 2H_2O$ (1). A mixture of A-α-PW_9 (0.237 g, 0.092 mmol), $CuCl_2\cdot 2H_2O$ (0.170 g, 1.000 mmol), en (0.10 mL, 1.480 mmol), and H_2O (5 mL, 278 mmol) was stirred for 4 h, sealed in a 20 mL Teflon-lined steel autoclave, kept at 120 °C for 5 days, and then cooled to room temperature. Blue prismatic crys-tals of **1** were obtained. Yield: ca. 28% (based on A-α-PW_9). Anal. Calcd (found %) for **1**: C, 3.38 (3.51); H, 1.49 (1.79); N, 3.94 (3.80).

$[Cu_6(\mu_3{-}OH)_3(en)_3(H_2O)_5(B\text{-}\alpha\text{-}PW_9O_{34})]\cdot 6H_2O$ (2). The process is similar to that of **1** with a mixture of of A-α-PW_9 (0.260 g, 0.101 mmol), $CuCl_2\cdot 2H_2O$ (0.128 g, 0.750 mmol), en (0.05 mL, 0.740 mmol), and H_2O (5 mL, 278 mmol). Green rhombus crystals of **2** were obtained. Yield: 32% (based on A-α-PW_9). Anal. Calcd (found %) for **2**: C, 2.37 (2.35); H, 1.62 (1.97); N, 2.76 (2.75).

$Na_6\{[Cu_6(\mu_3{-}OH)_3(en)_3(H_2O)_2(B\text{-}\alpha\text{-}PW_9O_{34})]_2[Cu_4(H_2O)_2(B\text{-}\alpha\text{-}PW_9O_{34})_2]\}\cdot 2H_2en\cdot 8H_2O$ (3). The process is similar to that of **1** with a mixture of A-α-PW_9 (1.122 g, 0.438 mmol), $CuCl_2\cdot 2H_2O$ (0.296 g, 1.736 mmol), en (0.15 mL, 2.220 mmol), and H_2O (10 mL, 556 mmol). Blue polyhedral crystals of **3** were obtained. Yield: 21% (based on A-α-PW_9). Anal. Calcd (found %) for **3**: C, 1.77 (1.44); H, 0.95 (1.29); N, 2.06 (1.71).

$[Cu_6(\mu_3{-}OH)_3(en)_3(H_2O)_3(B\text{-}\alpha\text{-}PW_9O_{34})]\cdot 4H_2O$ (4). The process is similar to that of **1** with a mixture of A-α-PW_9 (0.510 g, 0.199 mmol), $CuCl_2\cdot 2H_2O$ (0.135 g, 0.792 mmol), en (0.05 mL, 0.740 mmol) and H_2O (5 mL, 278 mmol). Green hexagonal crystals of **4** were obtained Yield: 36% (based on A-α-PW_9). Anal. Calcd (found %) for **4**: C, 2.43 (2.39); H, 1.39 (1.86); N, 2.83 (2.83).

$[Cu^{II}_6Cu^{I}_4(\mu_6\text{-}O)(OH)_{18}][Cu_6(\mu_3{-}OH)_3(enMe)_3(H_2O)_3(B\text{-}\alpha\text{-}PW_9O_{34})]_4\cdot 4H_3O\cdot 2H_2O$ (5). A mixture of A-α-PW_9 (0.475 g, 0.185 mmol), $CuCl_2\cdot 2H_2O$ (0.135 g, 0.792 mmol), enMe (0.05 mL, 0.589 mmol), Na_2CO_3 (0.20 mL, 1 mol L^{-1}), and H_2O (5 mL, 278 mmol) was stirred for 4 h, sealed in a 20 mL Teflon-lined bomb, kept at 120 °C for 5 days, and then cooled to room temperature. Cyan cubic crystals of **5** were obtained. Yield: 15% (based on A-α-PW_9). Anal. Calcd (found %) for **5**: C, 3.38 (3.68); H, 1.18 (1.69); N, 2.63 (2.49).

Single-Crystal Structure Determination. A single-crystal was mounted on a glass fiber for indexing and intensity data were collected at 293 K on Rigaku Saturn 70 CCD diffractometer for

(4) (a) Zheng, S.-T.; Yuan, D.-Q.; Jia, H.-P.; Zhang, J.; Yang, G.-Y. *Chem. Commun.* **2007**, 1858. (b) Zheng, S.-T.; Zhang, J.; Yang, G.-Y. *Angew. Chem., Int. Ed.* **2008**, *47*, 3909. (c) Zhao, J.-W.; Jia, H.-P.; Zhang, J.; Zheng, S.-T.; Yang, G.-Y. *Chem.—Eur. J.* **2007**, *13*, 10030. (d) Zhao, J.-W.; Zhang, J.; Song, Y.; Zheng, S.-T.; Yang, G.-Y. *Eur. J. Inorg. Chem.* **2008**, 3809.

(5) (a) Zheng, S.-T.; Wang, M.-H.; Yang, G.-Y. *Chem. Asian J.* **2007**, *2*, 1380. (b) Wang, J.; Du, X.; Niu, J. *Chem. Lett.* **2006**, *35*, 1408.

(6) (a) Zheng, S.-T.; Yuan, D.-Q.; Zhang, J.; Yang, G.-Y. *Inorg. Chem.* **2007**, *46*, 4569. (b) Zhao, J.-W.; Zheng, S.-T.; Li, Z.-H.; Yang, G.-Y. *Dalton Trans.* **2009**, 1300.

(7) (a) Zhao, J.-W.; Zhang, J.; Zheng, S.-T.; Yang, G.-Y. *Chem. Commun.* **2008**, 570. (b) Zhao, J.-W.; Wang, C.-M.; Zhang, J.; Zheng, S.-T.; Yang, G.-Y. *Chem.—Eur. J.* **2008**, *14*, 9223.

Table 1. X-ray Crystallographic Data for **1**−**5**

	1	**2**	**3**	**4**	**5**
formula	$C_{16}H_{84}Cu_9N_{16}O_{78}P_2W_{18}$	$C_6H_{49}Cu_6N_6O_{48}PW_9$	$C_{16}H_{102}Cu_{16}N_{16}Na_6O_{154}P_4W_{36}$	$C_6H_{41}Cu_6N_6O_{44}PW_9$	$C_{36}H_{150}Cu_{34}N_{24}O_{185}P_4W_{36}$
fw	5692.00	3040.37	10880.20	2968.31	12782.64
crystal system	monoclinic	monoclinic	monoclinic	monoclinic	cubic
space group	$P\bar{1}$	$P2_1/m$	$P2_1/n$	$P2_1/n$	$P\bar{4}3n$
a (Å)	13.380(3)	11.200(3)	20.568(7)	12.049(2)	22.8152(11)
b (Å)	13.625(3)	17.370(4)	20.773(7)	18.575(3)	22.8152(11)
c (Å)	16.608(3)	13.969(3)	24.028(9)	20.811(3)	22.8152(11)
α	71.954(6)	90	90	90	90
β (deg)	72.091(6)	94.422(4)	113.1(1)	94.1(1)	90
γ	89.904(8)	90	90	90	90
V (Å^3)	2724.6(10)	2709.5(1)	9445(6)	4646.0 (1)	11876.1(10)
Z	1	2	2	4	2
d_{calcd} (g cm^{-3})	3.469	3.727	3.826	4.244	3.575
cryst size (mm^3)	0.11 × 0.09 × 0.03	0.24 × 0.12 × 0.07	0.16 × 0.06 × 0.06	0.18 × 0.08 × 0.07	
index range	$-17 \le h \le 17$ $-15 \le k \le 17$ $-21 \le l \le 21$	$-14 \le h \le 14$ $-22 \le k \le 12$ $-18 \le l \le 18$	$-24 \le h \le 24$ $-24 \le k \le 14$ $-28 \le l \le 28$	$-15 \le h \le 12$ $-24 \le k \le 23$ $-26 \le l \le 27$	$-27 \le h \le 29$ $-29 \le k \le 27$ $-29 \le l \le 22$
no. of measured reflns	21253	19906	56342	33354	87108
no. of unique reflns	12213	6384	16400	10530	4433
R_{int}	0.0344	0.0502	0.0511	0.0364	0.0464
wavelength (Å)	0.71073	0.71073	0.71073	0.71073	0.71073
abs coeff (mm^{-1})	20.749	21.455	23.725	25.013	20.450
GOF on F^2	1.033	1.061	1.085	1.020	1.082
R_1[a] [$I > 2\sigma(I)$]	0.0435	0.0366	0.0838	0.0239	0.0396
wR_2[b] [$I > 2\sigma(I)$]	0.0994	0.0925	0.2001	0.0604	0.1009
R_1[a] (all data)	0.0551	0.0462	0.0962	0.0322	0.0400
wR_2[b] (all data)	0.1082	0.0972	0.2082	0.0858	0.1013

[a] $R_1 = \Sigma||F_o| - |F_c||/\Sigma|F_o|$. [b] $wR_2 = [\Sigma w(F_o^2 - F_c^2)^2/\Sigma w(F_o^2)^2]^{1/2}$; $w = 1/[\sigma^2(F_o^2) + (xP)^2 + yP]$, $P = (F_o^2 + 2F_c^2)/3$, where $x = 0.0585$, $y = 0.0000$ for **1**; $x = 0.0496$, $y = 0.0000$ for **2**; $x = 0.0746$, $y = 754.4212$ for **3**; $x = 0.0550$, $y = 0.0000$ for **4**; and $x = 0.0551$, $y = 223.4038$ for **5**.

1−**5** with graphite-monochromated Mo Kα ($\lambda = 0.71073$ Å). Direct methods were used to solve the structures and to locate the heavy atoms using the SHELXTL-97 program package.[8] The remaining atoms were found from successive full-matrix least-squares refinements on F^2 and Fourier syntheses. Routine Lorentz polarization corrections and empirical absorption correction were applied to intensity data. No hydrogen atoms associated with water molecules were located from the difference Fourier map. Hydrogen atoms attached to carbon and nitrogen atoms were geometrically placed. All hydrogen atoms were refined isotro-pically as a riding mode using the default SHELXTL parameters. For **1**, all non-H atoms were refined anisotropically except for three free water molecules (OW5-OW7), seven carbon atoms (C2, C2′, C3, C3′, C5−C7) and three nitrogen atoms (N2, N6, N8). The C2 and C3 atoms were disordered over two positions, with the site occupation factors of 0.35/0.65 for C2/C2′ and 0.5/0.5 for C3/C3′, respectively. For **2**, all non-H atoms were refined anisotropically except for the three water molecules (OW5-OW7). The N4 atom was disordered over two positions with the site occupation factors of 0.25/0.25 for N4/N4′. For **3**, all non-H atoms were refined anisotropically except for six water molecules (OW1−OW4, OW6−OW7), four carbon atoms (C3, C6−C8), two nitrogen atoms (N3, N7), a sodium atom (Na1), and two oxygen atoms (O67 and O71). The W10, W11, W14, W15, W17, W18 atoms were disordered over two positions with the site occupation factors of 0.9/0.1 for W10/W10′, W11/W11′, W14/W14′, W15/ W15′, and W18/W18, as well as 0.88/0.12 for W17/W17, respectively. For **4**, all non-H atoms were refined anisotropically, except for two free water molecules (O1W and O7W). CCDC-673186, 673183, 673184, 673185, and 688252 contains the supplementary crystallographic data for **1**, **2**, **3**, **4**, and **5** in this paper. Further details for structural analyses of **1**−**5** are summarized in Table 1.

(8) Sheldrick G. M. *SHELXS97, Program for Crystal Structure Solution*; University of Göttingen: Göttingen, Germany, 1997.

Results and Discussions

Syntheses. At the beginning of our launching the strategy that using the lacunary sites of trivacant Keggin fragments as structure-directing agents induce the formation of high-nuclear TM oligomers and organoamines as structure-stabilizing agents capture and stabilize in situ formed TM oligomers to further construct novel TMSPs, we first obtained a family of hexa-Ni substituted POTs.[4] These interesting findings enlighten us to explore the system containing A-α-PW_9, $CuCl_2 \cdot 2H_2O$ and en. Fortunately, we first isolated the hexa-Cu^{II} substituted $[Cu_6(en)_3(H_2O)_3]\{B\text{-}\alpha\text{-}PW_9O_{34}\}] \cdot 7H_2O$ (**6**).[4c] With our continuous efforts, **1**−**5** were successively isolated. In fact, during the course of exploitation, we also made a mono-Cu^{II} substituted Keggin POT, $[Cu(en)_2(H_2O)]_2\{[Cu(en)_2][\alpha\text{-}PCuW_{11}O_{39}Cl]\} \cdot 3H_2O$ (**7**).[9] To compare with the synthetic conditions of **1**−**7**, their formation is chiefly controlled by the A-α-PW_9O_{34}/Cu^{2+} molar ratio and the pH value. When the A-α-PW_9O_{34}/Cu^{2+} molar ratio is larger and the pH value is higher, the formation of hexa-Cu^{II} substituted POTs is favorable. On contrast, the smaller A-α-PW_9O_{34}/Cu^{2+} molar ratio and the lower pH value tends to the formation of mono-Cu^{II} substituted Keggin POTs.

Considering the similarities between A-α-PW_9O_{34} and A-α-SiW_9O_{34}/A-α-GeW_9O_{34}, the systems containing A-α-SiW_9O_{34}/A-α-GeW_9O_{34}, $CuCl_2 \cdot 2H_2O$, and en/enMe were also investigated. Experimental results reveal that the larger molar ratio of A-α-XW_9O_{34}/Cu^{2+} ($X = Si^{IV}/Ge^{IV}$) favors to form octa-Cu^{II} sandwiched POTs,[4c,7] whereas the smaller molar ratio of A-α-XW_9O_{34}/Cu^{2+}

(9) Zhao, J.-W.; Zhang, J.; Zheng, S.-T.; Yang, G.-Y. *J. Solid State Chem.* **2008**, *181*, 2205.

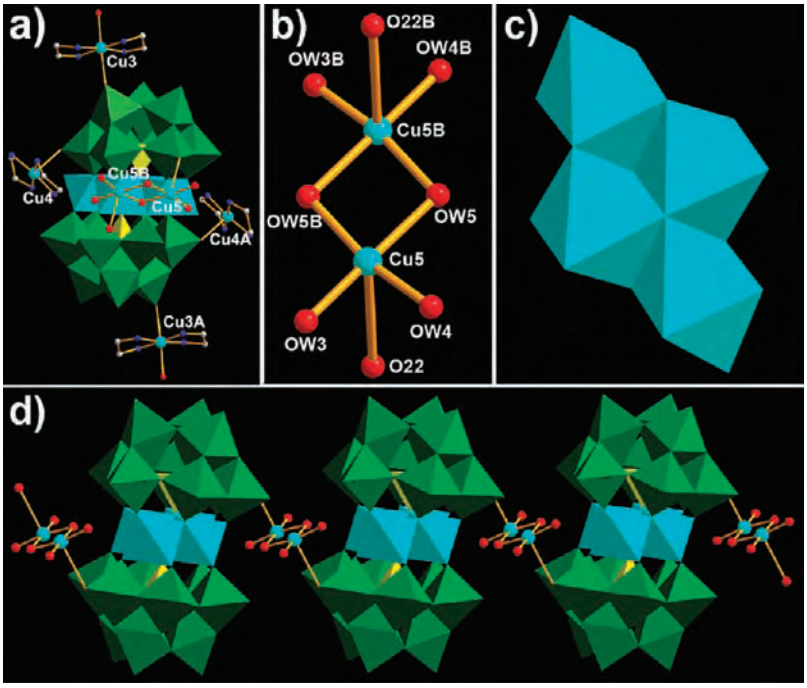

Figure 1. (a) Combined polyhedral/ball-and-stick representation of the decorated $[Cu_4(H_2O)_2(\mathbf{PW_9})_2]^{10-}$; (b) coordination environment of the $[Cu_2(H_2O)_6]^{4+}$ dimer; (c) polyhedral representation of the tetra-Cu cluster in **1**; (d) 1D chain of **1**. The symmetry codes: A $-x + 1, -y + 1, -z + 1$; B $-x + 2, -y + 1, -z + 1$.

tends to form mono-Cu^{II} substituted Keggin POTs.[9] In a word, the nature differences of A-α-PW_9O_{34} and A-α-SiW_9O_{34}/A-α-GeW_9O_{34} lead to the structural distinctions of the resulting products.

Notice that the A-α-PW_9O_{34} unit as a starting material was transformed to the B-α-PW_9O_{34} unit in all the products, indicating that the isomerization of A-α-PW_9O_{34} → B-α-PW_9O_{34} must have taken place during the course of the reactions. This isomerization of A-α-PW_9O_{34} → B-α-PW_9O_{34} may be closely related to the reaction conditions and the stability of the resulting compounds. On one hand, when the reaction is carried out under heating condition, it is favorable for this isomerization of A-α-PW_9O_{34} → B-α-PW_9O_{34}, which is in good agreement with the driving force of isomerization controlled by the thermodynamic factors.[10] On the other hand, the A-α-PW_9O_{34} unit has six exposed surface oxygen atoms in the vacant site, whereas the B-α-PW_9O_{34} unit has seven exposed surface oxygen atoms in the vacant site; therefore, the B-α-PW_9O_{34} unit can work as a heptadentate ligand to coordinate to the generated in situ Cu^{II} clusters and further enhance the stability of the resulting products.

Structure of $[Cu(en)_2]_2[Cu(en)_2(H_2O)]_2[Cu(H_2O)_2][Cu_4(H_2O)_2(B\text{-}\alpha\text{-}PW_9O_{34})_2]\cdot 2H_2O$ (1). **1** consists of a tetra-Cu^{II} sandwiched polyoxoanion $[Cu^{II}_4(H_2O)_2(\mathbf{PW_9})_2]^{10-}$ decorated by two $[Cu^{II}(en)_2]^{2+}$ and two $[Cu^{II}(en)_2(H_2O)]^{2+}$ groups (Figure 1a), and half dicopper $[Cu^{II}_2(H_2O)_6]^{4+}$ dimer (Figure 1b). The centrosymmetric $[Cu_4(H_2O)_2(\mathbf{PW_9})_2]^{10-}$ unit contains two trivacant Keggin $\mathbf{PW_9}$ fragments linked together by a centrosymmetric tetra-metallic unit $Cu^{II}_4O_{16}$ (Figure 1c) to form a sandwich-type structure. The first sandwiched phosphotungstate $[Co_4(H_2O)_2(\mathbf{PW_9})_2]^{10-}$ was reported by Weakley et al. by the reaction of a 11:2:4:18 mixture of $HCl/Na_2HPO_4/Co(NO_3)_2/Na_2WO_4$ at 90−100 °C in 1973.[11] Later, almost all TM-substituted analogues have been reported under conventional aqueous solution method and become rapidly the largest subfamily of POMs. Most of these structures are discrete and purely inorganic compounds. Lately, a amount of organic−inorganic composite based on $\{TM_4(L)_2(\mathbf{PW_9})_2\}$ (L = H_2O or amine) have been isolated under hydrothermal conditions. These hybrids are multidimensional frameworks bridging by mononuclear TM complexes or rare-earth ions.[5,12] Compared with above-mentioned organic−inorganic architectures, the most remarkable feature of **1** is a 1D chain built up from $[Cu_4(H_2O)_2(\mathbf{PW_9})_2]^{10-}$ and dinuclear $[Cu_2(H_2O)_6]^{4+}$ units (Figure 1d). In comparison with 1D chainlike organic−inorganic POM $[Cu(en)_2]_3[Cu(en)_2(H_2O)]_2\{[Cu_4(GeW_9O_{34})_2][Cu(en)_2]\}\cdot 9.5\,H_2O$ (**8**),[5b] four obvious differences between them are observed: (1) both POM units are different, [B-α-PW_9O_{34}]$^{9-}$ for **1** and [B-α-GeW_9O_{34}]$^{10-}$ for **8**; (2) the tetra-Cu cluster in **1** has two coordinated water ligands whereas there is no water ligand in the tetra-Cu cluster in **8**; (3) the 1D chain of **1** is made by $[Cu_4(H_2O)_2(B\text{-}\alpha\text{-}PW_9)_2]^{10-}$ and dinuclear $[Cu_2(H_2O)_6]^{4+}$ units; in contrast, the 1D chain in **8** is built by the $[Cu_4(B\text{-}\alpha\text{-}GeW_9O_{34})_2]^{12-}$ and mononuclear $[Cu(en)_2]^{2+}$ units; 4) the pseudo-Jahn−Teller effect of the CuO_5 square pyramid plays an important role in the formation of 1D chain of **1**, whereas the Jahn−Teller effect of CuN_4O_2 octahedra is responsible for the construction of 1D chain in **8**. The dinuclear $[Cu_2(H_2O)_6]^{4+}$ bridging mode in **1** is rare in POM chemistry and each Cu^{II} ion adapts the square

(10) (a) Kortz, U.; Mbomekalle, I. M.; Keita, B.; Nadjo, L.; Berthet, P. *Inorg. Chem.* **2002**, *41*, 6412. (b) Domaille, P. J. *Inorg. Synth.* **1990**, *27*, 96.

(11) Weakley, T. J. R.; Evans jun, H. T.; Showell, J. S.; Tourné, G. F.; Tourné, C. M. *J. Chem. Soc. Chem. Commun.* **1973**, 139.

(12) Li, Y.-G.; Chen, W.-L.; Wang, E.-B.; Wang, X.-L. *Inorg. Chem. Commun.* **2008**, *11*, 879.

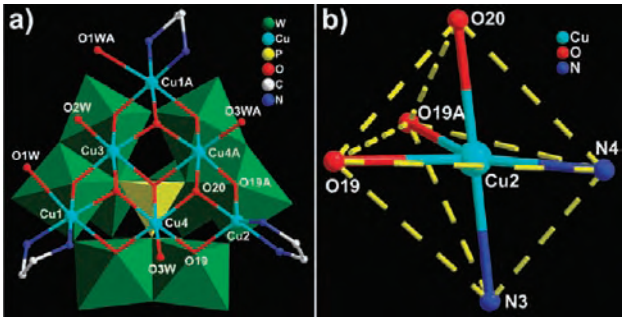

Figure 2. (a) Combined polyhedral/ball-and-stick representation of **2**; (b) distorted trigonal bipyramid of $Cu2O_3N_2$ with the Cu−O/N distances are as follows: Cu(2)−O(19,19A) 2.159(6), Cu(2)−O(20) 1.971(9), Cu-(2)−N(3) 2.01(2), and Cu(2)−N(4) 1.94(4) Å. The symmetry code: A x, $-y + 1/2$, z.

pyramid geometry in which the basal positions are occupied by four O atoms from four water ligands (Cu−O, 1.92(3)−2.189(17) Å) and the axial position is occupied by an oxygen ligand from the polyoxoanion $[Cu_4(H_2O)_2(\mathbf{PW_9})_2]^{10-}$ (Cu−O, 2.826(9) Å).

Structure of $[\mathbf{Cu_6}(\mu_3\text{−}\mathbf{OH})_3(\mathbf{en})_3(\mathbf{H_2O})_5(\mathbf{B}\text{-}\alpha\text{-}\mathbf{PW_9O_{34}})]\cdot\mathbf{6H_2O}$ (2). 2 crystallizes in the monoclinic space group $P2_1/m$. The molecular structure of **2** consists of a trivacant Keggin unit $\mathbf{PW_9}$ and a hexa-Cu cluster $\{\mathbf{Cu_6}(en)_3(H_2O)_5\}$(Figure 2a and Figure S1 in the Supporting Information). It should be noted that this $\{\mathbf{Cu_6}(en)_3(H_2O)_5\}$ cluster, which is induced by $\mathbf{PW_9}$ unit, is built by six coplanar Cu^{II} ions in a triangle motif by three μ_3−OH bridges (Cu−μ_3−O_{OH}, 1.971(9)−2.034(6) Å), and then stabilized by six μ_3−O bridges from the lacunae of $\mathbf{PW_9}$ unit (Cu−μ_3−O, 1.969(6)−2.355(6) Å) and one μ_4−O bridge from the central PO_4 unit [Cu−μ_4−O: 2.249 (8)−2.265(6) Å]. Different from the reported hexa-Ni^{II} substituted POTs and **6**,[4] a mirror passing through Cu2 and Cu3 atoms in **2** lead to the occurrence of two types of coordination geometries of six Cu^{II} ions. Five of them (Cu1, Cu1A, Cu3, Cu4, Cu4A) inhabit in the octahedral geometry completed by three oxygen atoms from the $\mathbf{PW_9}$ unit, one en, and one water ligand, whereas one (Cu2) possesses a trigonal bipyramidal geometry constituted by three oxygen atoms from the $\mathbf{PW_9}$ unit and one en ligand (Figure 2b). To date, such trigonal bipyramidal geometry is not found in Ni-polyhedra of $\mathbf{Ni_6}$ core.[4]

In addition to the coplanar hexa-Cu clusters in **2** and **6**, another two types of coplanar hexa-Cu clusters are also observed in two sandwiched POTs $[Cu_6Cl_6(B\text{-}\alpha\text{-}AsW_9O_{33})_2]^{12-}$ (**9**)[13] and $[Cu\text{-}(enMe)_2]_2\{[Cu(enMe)_2(H_2O)]_2[Cu_6(enMe)_2(B\text{-}\alpha\text{-}SiW_9O_{34})_2]\}\cdot 4H_2O$ (**10**),[6a] which were reported by Yamase's and our group in 2006 and 2007, respectively. Compared coplanar hexa-Cu clusters in the sandwiched POTs with hexa-Cu cluster in **2**, their linking modes of Cu^{II} cations are different (Figure 3). In **9**, the hexa-Cu cluster with D_{3d} symmetry shows a hexagonal ring by the edge-sharing linking mode (Figure 3a) and each Cu^{II} ion exhibits the square-pyramid geometry, whose equatorial plane is defined by four O atoms from two $[B\text{-}\alpha\text{-}AsW_9O_{33}]^{9-}$ fragments and an exterior Cl^- ion is situated on the apex position. In **10**, the hexa-Cu cluster with the C_i symmetry

(13) Yamase, T.; Fukaya, K.; Nojiri, H.; Ohshima, Y. *Inorg. Chem.* **2006**, *45*, 7698.

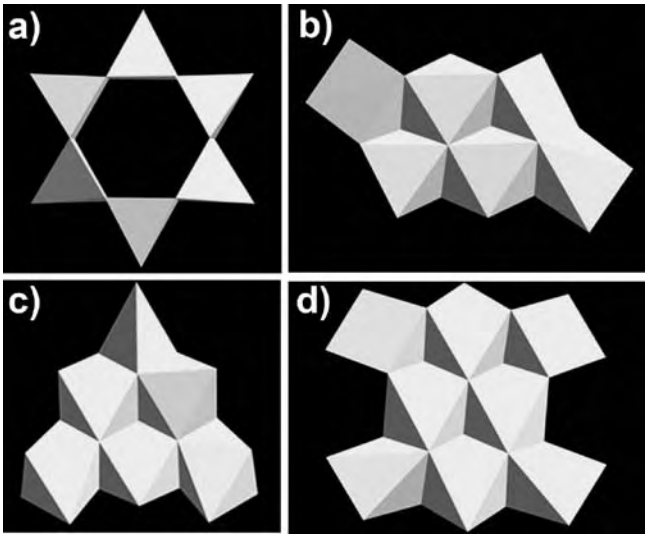

Figure 3. Polyhedral representations of the connection fashion of the coplanar hexa-/octa-Cu clusters: (a) hexa-Cu cluster in **9**; (b) hexa-Cu cluster in **10**; (c) hexa-Cu cluster in **2**; (d) octa-Cu cluster in refs 4c and 7.

exhibits a beltlike arrangement generated by the edge-sharing mode (Figure 3b), in which there are three kinds of Cu^{II} coordination environments, two central Cu^{II} ions are octahedrally coordinated by six O atoms from two $[B\text{-}\alpha\text{-}SiW_9O_{34}]^{10-}$ fragments, two Cu^{II} ions are square-pyramidally coordinated by five O atoms from two $[B\text{-}\alpha\text{-}SiW_9O_{34}]^{10-}$ fragments, and two Cu^{II} ions are also square-pyramidally coordinated by three O atoms from two $[B\text{-}\alpha\text{-}SiW_9O_{34}]^{10-}$ fragments and two N atoms from enMe ligands, whereas in **2**, the connection of six coplanar Cu^{II} ions shows the edge-sharing mode with a triangle distribution (Figure 3c). Very recently, a family of octa-Cu cluster sandwiched POTs have been reported by our lab.[4c,7] The almost coplanar eight Cu^{II} cations are arranged in the motif of 3:2:3 (Figure 3d), and the octa-Cu cluster $\{[Cu(L)]_4Cu_4O_{14}(H_2O)_2\}$ (L = en/enMe/2,2′-bpy) can also be considered as four exogenous five-coordinate $[Cu(L)]^{2+}$ cations grafting to four corners of the rhombic cluster $\{Cu_4O_{14}(H_2O)_2\}$ in **1** through twelve oxygen atoms from two trivacant $\mathbf{PW_9}$ fragments. However, the coplanar hexa-/octa-Cu sandwiched phosphotungstates have not been observed in POM chemistry because of the different nature of radius and charge of the centeral $P^V/Si^{IV}/Ge^{IV}$ heteroatoms.

Structure of $\mathbf{Na_6}\{[\mathbf{Cu_6}(\mu_3\text{−}\mathbf{OH})_3(\mathbf{en})_3(\mathbf{H_2O})_2(\mathbf{B}\text{-}\alpha\text{-}\mathbf{PW_9O_{34}})]_2[\mathbf{Cu_4}(\mathbf{H_2O})_2(\mathbf{B}\text{-}\alpha\text{-}\mathbf{PW_9O_{34}})_2]\}\cdot\mathbf{2H_2en}\cdot\mathbf{8H_2O}$ (3). 3 is an unprecedented inorganic−organic hybrid doubly sandwiched POT and its main backbone (Figure 4a) is composed of two identical hexa-Cu substituted POT units $\{\mathbf{Cu_6}(en)_3(H_2O)_2(\mathbf{PW_9})\}$ (**3a**, Figure 4b and Figure S2 in the Supporting Information) and a tetra-Cu sandwiched POT unit $\{Cu_4(H_2O)_2(\mathbf{PW_9})_2\}$[14] (**3b**, Figure 4c). The $\{\mathbf{Cu_6}(en)_3(H_2O)_2\}$ unit in **3a** is somewhat different from the $[\mathbf{Cu_6}(en)_3(H_2O)_5]$ unit in **2**. The hexa-Cu cluster in **2** contains one CuN_2O_3 trigonal bipyramid, two CuN_2O_4 octahedra, and three CuO_6 octahedra, whereas the hexa-Cu cluster in **3a** consists of one CuN_2O_3 square pyramid (Figure 4d), one Cu N_2O_3 trigonal bipyramid (Figure 4e), one CuN_2O_4 octahedron, and three CuO_6 octahedra, (Figure 4f,g). The pentacoordinated CuN_2O_3 square

(14) Finke, R. G.; Droege, M. *J. Am. Chem. Soc.* **1981**, *103*, 1587.

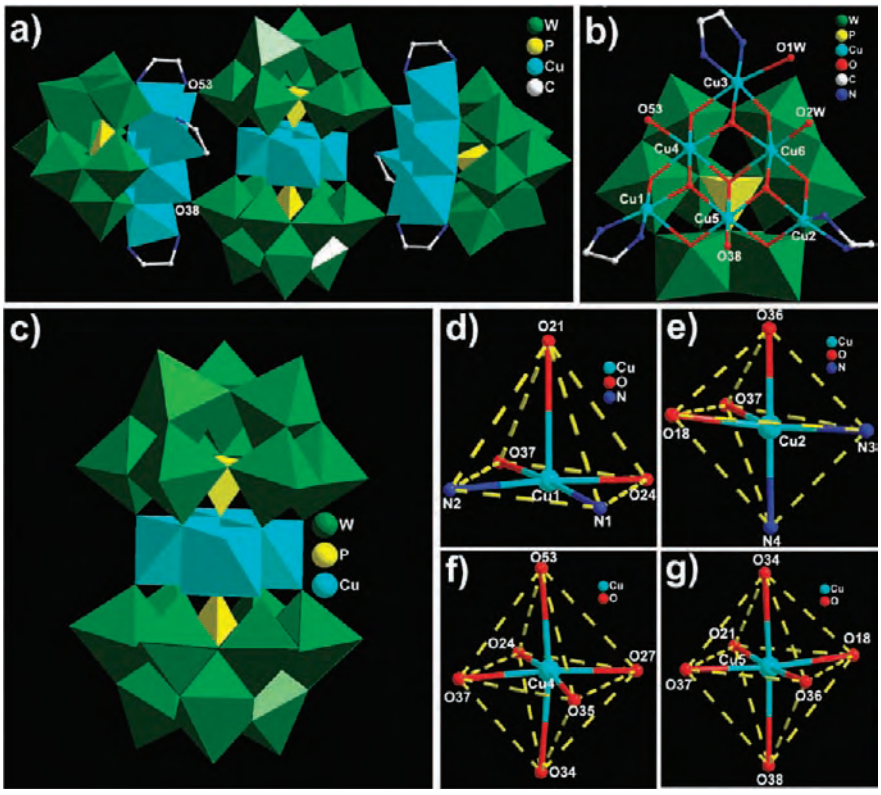

Figure 4. (a) Double sandwich-type representation of **3**; (b) combined ball-and-stick/polyhedral view of **3a**; (c) polyhedral view of **3b**. (d) $Cu1O_3N_2$ square pyramid: Cu1−O21 2.42(2), Cu1−O24 2.00(2), Cu1−O37 1.991(17), Cu1−N1 2.04(2). and Cu1−N2 2.00(2) Å. (e) $Cu2O_3N_2$ trigonal bipyramid: Cu2−O18 2.073 (18), Cu2−O33 2.350(19), Cu2−O36 1.981(18), Cu2−N3 1.99(4), and Cu2−N4 2.02(3) Å. (f) $Cu4O_6$ axial elongation octahedron: Cu4−O27 1.954(17), Cu4−O37 2.000(16), Cu4−O35 2.044(18), Cu4−O24 2.088(17), Cu4−O34 2.254(16), and Cu4−O53 2.28(2) Å. (g) $Cu5O_6$ axial elongation octahedron: Cu5−O21 1.971 (18), Cu5−O18 2.03(2), Cu5−O36 2.030(17), Cu5−O37 2.053(18), Cu5−O34 2.194(16), and Cu5−O38 2.208(19) Å.

pyramids in **2** and **3a** are all situated on the "corner" sites of the triangle. According to both structural characteristics, of special interest is that **3** can be viewed as a derivative of **2** by means of participation of the tetra-Cu sandwiched POT unit $[Cu_4(H_2O)_2(\mathbf{PW_9})_2]^{10-}$. Specifically, four terminal O atoms of two $\mathbf{PW_9}$ in **3b** substitute four water ligands of two $\{\mathbf{Cu_6}(en)_3(H_2O)_2\}$ units of two **3a**, resulting in a novel duple sandwich-type assembly, that is, the tetra-Cu sandwiched-type **3b** is further sandwiched by two **3a**. Such linkage modes are unique in POM and coordination chemistry. Interestingly, two water ligands on two interior Cu(4,5) atoms of the triangular $\mathbf{Cu_6}$ cluster in **3a** were simultaneously substituted by two terminal O(38,53) atoms from a big-size **3b** unit. Why can the substitution reaction take place in **3**? It may be attributed to two major reasons: (1) The steric hindrance of two penta-coordinated $Cu(1,2)O_3N_2$ polyhedra is much less than that of expected two six-coordinated $Cu(1,2)O_3N_2(H_2O)$ octahedra. (2) The Jahn−Teller effect results in the axial elongation of $Cu(4,5)O_6$ octahedra (Figure 4f,g), which can further reduce or overcome large steric hindrance when big **3b** unit attacks two **3a** units. These two factors favor to the occurrence of the above substitution reaction to some extent. This phenomenon can also be viewed as a "synergistic effect" between the distortion of the polyhedra (trigonal bipyramid and square pyramid) and the Jahn−Teller effect of the octahedra with the axial elongation. It is noteworthy that such a substitution has not been observed in Ni^{II}-octahedra of the $\mathbf{Ni_6}$ core.[4] From the above analysis, **3** may experience a two-step process: the formation of **3a** and **3b** units, and then further combination of **3a** and **3b** (see Figure S3 in the Supporting Information). As a matter of fact, the analogous intermediates **1** and **2** have been captured under the similar conditions, which partly support our hypothesis that **3** may experience a two-step combination process. Similar reports in which some intermediates have been successfully trapped by hydro(solvo)thermal techniques are rare.[15] This can help us to better understand the mysterious equilibrium of the formation of some POMs, so that eventually rational syntheses of novel species may be possible. To the best of our knowledge, **3** is the first tetramer containing two different TMSP units in POM chemistry that differs from those reported tetramers containing four same TMSP units: $[\{(SiW_9O_{34})(SiW_9O_{33}(OH))(Cu(OH))_6Cu\}_2X]^{23-}$ (X = Cl/Br), $[\{Fe^{II}_{1.5}Fe^{III}_{12}(\mu_3-OH)_{12}(\mu_4-PO_4)_4\}(B-\alpha-PW_9O_{34})_4]^{21-}$, $[Nb_4O_6(\alpha-Nb_3SiW_9O_{40})_4]^{20-}$, $[\{\beta-Ti_2SiW_{10}O_{39}\}_4]^{24-}$, $[Cu_{14}(OH)_4(H_2O)_{16}(SiW_8O_{31})_4]^{16-}$, $[Cu_{10}(H_2O)_2(N_3)_4(GeW_9O_{34})_2(GeW_8O_{31})_2]^{24-}$, $[\{(B-\alpha-PW_9O_{34})Fe_3(OH)_3\}_4(PO_4)_4Fe]^{22-}$, $[(\alpha-PW_{10}Fe_2O_{39})_4]^{28-}$, $[\{Fe^{II}Fe^{III}_{12}(\mu_3-OH)_{12}(\mu_4-PO_4)_4\}(B-\alpha-PW_9O_{34})_4]^{22-}$.[4c,16]

(15) (a) Zhang, J. P.; Lin, Y. Y.; Huang, X. C.; Chen, X. M. *J. Am. Chem. Soc.* **2005**, *127*, 5495. (b) Chen, X.-M.; Tong, M. L. *Acc. Chem. Res.* **2007**, *40*, 162.

(16) (a) Kim, G. S.; Zeng, H.; VanDerveer, D.; Hill, C. L. *Angew. Chem., Int. Ed.* **1999**, *38*, 3205. (b) Hussain, F.; Bassil, B. S.; Bi, L.; Reicke, M.; Kortz, U. *Angew. Chem., Int. Ed.* **2004**, *43*, 3485. (c) Pichon, C.; Dolbecq, A.; Mialane, P.; Marrot, J; Rivière, E.; Sécheresse, F. *Dalton Trans.* **2008**, 71. (d) Pradeep, C. P.; Long, D.-L.; Kögerlerb, P.; Cronin, L. *Chem. Commun.* **2007**, 4254. (e) Kortz, U.; Hamzeh, S. S.; Nasser, N. A. *Chem.—Eur. J.* **2003**, *9*, 2945. (f) Godin, B.; Chen, Y.; Vaissermann, J.; Ruhlmann, L.; Verdaguer, M.; Gouzerh, P. *Angew. Chem., Int. Ed.* **2005**, *44*, 3072. (g) Mialane, P.; Dolbecq, A.; Marrot, J.; Rivière, E.; Sécheresse, F. *Angew. Chem., Int. Ed.* **2003**, *42*, 3523.

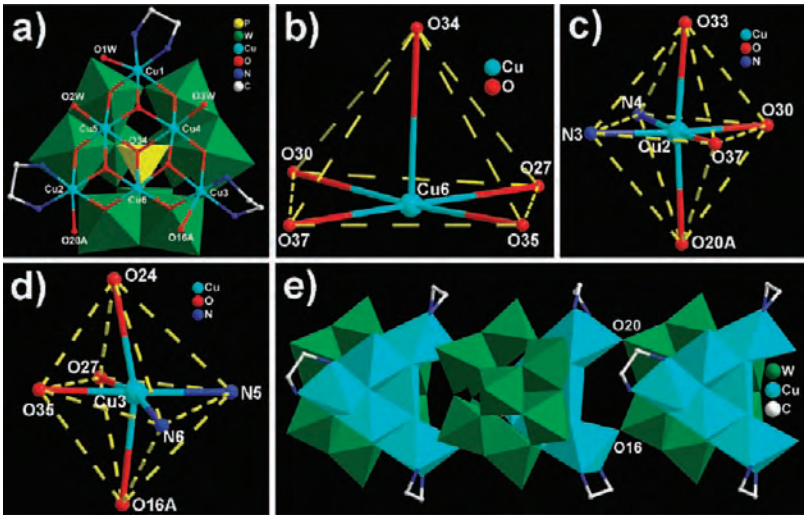

Figure 5. (a) Combined ball-and-stick/polyhedral view of **4**. (b) $Cu6O_5$ square pyramid: Cu6−O37 1.929(5), Cu6−O27 1.948(5), Cu6−O(30) 1.982(5), Cu6−O35 1.989(5), Cu6−O34 2.267(6) Å. (c, d) Axial elongation octahedra of $Cu2N_2O_4$ and $Cu3N_2O_4$: Cu2−O37 1.968(5), Cu2−N4 1.991(7), Cu2−N3 2.012(7), Cu2−O30 2.032(5), Cu2−O33 2.470(7), Cu2−O20A 2.497(7) Å, Cu3−O35 1.988(5), Cu3−N5 1.993(7), Cu3−N6 1.999(7), Cu3−O27 2.008(5), Cu3−O24 2.369(6), and Cu3−O16A 2.425(6) Å; (e) 1D chain of **4**. The symmetry code: A $-x-1/2$, $y-1/2$, $-z+1/2$.

Structure of $[Cu_6(\mu_3-OH)_3(en)_3(H_2O)_3(B\text{-}\alpha\text{-}PW_9O_{34})]\cdot 4H_2O$ (4). Different from the hexa-Cu units in **2** and **3**, the $\{Cu_6(en)_3(H_2O)_3\}$ unit in **4** contains one CuO_5 square pyramid, two CuO_6 octahedra and three CuN_2O_4 octahedra (Figure 5a and Figure S4 in the Supporting Information). Because of the pseudo-Jahn−Teller effect of $Cu6O_5$ square pyramid (Figure 5b), the steric hindrance of the $Cu6O_5$ square pyramid is less than that of the $Cu6O_5$-(H_2O) octahedron; Additionally, the Jahn−Teller effect of $Cu(2,3)O_4N_2$ octahedra with the axial elongation (Figure 5c,d) further reduce large steric hindrance when big $\{Cu_6PW_9$-$(en)_3(H_2O)_3\}$ SBU attack each other during substitution process, i.e., both the Jahn−Teller effect of $Cu(2,3)O_4N_2$ octahedra with the axial elongation and the pseudo-Jahn−Teller effect of $Cu6O_5$ square pyramid can reduce large steric hindrance when big $\{Cu_6PW_9$-$(en)_3(H_2O)_3\}$ SBUs are further polymerized together. Therefore, the "synergistic effect" between the pseudo-Jahn−Teller effect of the square pyramid and the Jahn−Teller effect of the octahedra just results in the case that two water ligands on two adjacent Cu2 and Cu3 atoms were simultaneously substituted by two terminal O16A and 20A atoms from same PW_9 fragment to form a novel linear chain 4 with double-bridging mode (Figure 5e), which differs from the single-bridging zigzag chain in Ni_6-based TMSP, $[Ni_6(\mu_3-OH)_3(H_2O)_2(dien)_3(B\text{-}\alpha\text{-}PW_9O_{34})]\cdot 4H_2O$.[4a] Therefore, the formation of **4** is driven by the Jahn−Teller/pseudo-Jahn−Teller effect of the Cu^{II}-polyhedra, whereas no such effect exists in the Ni^{II}-polyhedra.

Structure of $[Cu^I_4Cu^{II}_6(\mu_6\text{-}O)(OH)_{18}][Cu_6(\mu_3-OH)_3$-$(enMe)_3(H_2O)_3(B\text{-}\alpha\text{-}PW_9O_{34})]_4\cdot 4H_3O\cdot 2H_2O$ (5). The 3D framework of **5** consists of two distinct SBUs, $\{Cu_6$-$PW_9(enMe)_3(H_2O)_3\}$ (**5a**, Figure 6a and Figure S5 in the Supporting Information) and $[Cu^I_4Cu^{II}_6(\mu_6\text{-}O)(OH)_{18}]^{4-}$ templates formed in situ (**5b**, Figure 6b,c). The $[Cu_6$-$(enMe)_3(H_2O)_3]$ unit in **5a** contains three $Cu^{II}O_6$ and three $Cu^{II}N_2O_4$ octahedra. Because of the Jahn−Teller effect, the Cu1/Cu1A/Cu1B atoms exhibit the axial elongation (Figure 6d) in $\{Cu_6PW_9(enMe)_3(H_2O)_3\}$ SBUs, which provides a precondition for the formation of the 3D framework of **5**. Moreover, such axial elongation reduces the steric hindrance and benefits the occurrence of the substitution reaction, resulting in an unprecedented open-framework with three types of channels marked **A**, **B**, and **C** with dimensions of 4.5 × 4.5, 6.3 × 6.3 and 7.7 × 7.7 Å (Figure 6e,f), in which the **5b** cluster, the carbon atoms of enMe ligands, and the lattice water molecules are filled, respectively (Figure 6g−i). In each **5a** SBU, not only are three water ligands of three Cu1 atoms substituted by three terminal O atoms from three PW_9 units on another three **5a** SBUs but also three terminal O atoms of the PW_9 unit on each **5a** SBU substitute three water ligands on three $\{Cu_6(enMe)_3(H_2O)_3\}$ units from adjacent three **5a** SBUs (see Figure S6 in the Supporting Information). Thus, each 5a SBU connects six such SBUs via six Cu−O−W linkages, constructing the 3D open-framework. Taking into account each **5a** SBU as a 6-connected node, the framework of 5 exhibits a 3D α-Po net (Figure 6j) with a Schläfli topological notation for $4^{12}6^3$ and a long vertex symbols is 4.4.4.4.4.4.4.4.4.4.4.6(4).6(4).6(4). Such linking modes were not been observed in the Ni_6-based TMSPs. Therefore, the formation of **5** can be ascribed to the Jahn−Teller effect of $Cu1O_4N_2$ octahedra with the axial elongation. So far, no such elongation was observed in Ni-octahedra.

Another striking feature of **5** is the in situ formed decametallic cluster **5b** (Figure 6b,c) that is located in the cage surrounded by eight adjacent **5a** SBUs, and interacted with four **5a** SBUs via H-bonding (Figure 6k) that is responsible for the stability of **5b**. To the best of our knowledge, **5b** is first mixed-valence decanuclear Cu−O inorganic cluster, although organic−inorganic mixed-valent polynuclear Cu−O clusters have been reported.[17] **5b** is built by an octahedral $[Cu^{II}_6(\mu_6\text{-}O)$-$(OH)_{18}]^{8-}$ $\{Cu_6\}$ core and four Cu^I ions with trigonal pyramidal geometries. The $\{Cu_6\}$ core is similar to the well-known Lindqvist anions M_6O_{19} built by six MO_6 octahedra edge-shared via a central μ_6-O atom such as

(17) Mukherjee, A.; Nethaji, M.; Chakravarty, A. R. *Angew. Chem., Int. Ed.* **2004**, *43*, 87.

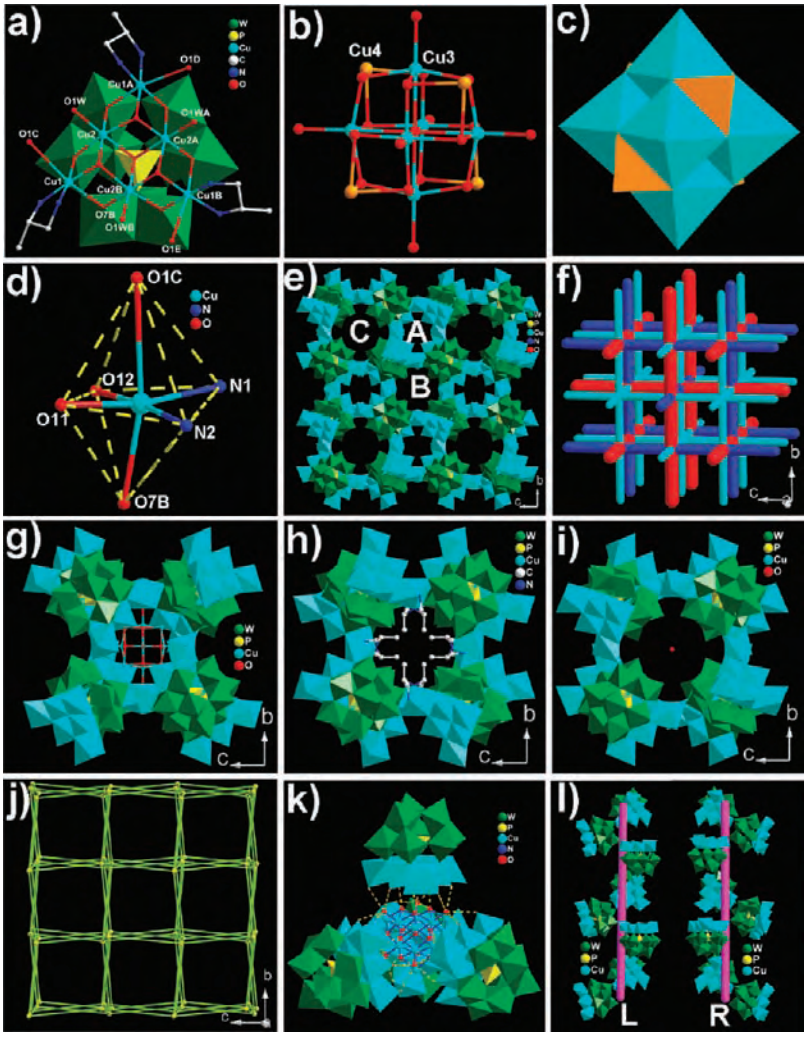

Figure 6. (a) Combined ball-and-stick/polyhedral representation of **5a**. (b, c) Ball-and-stick/polyhedral representations of **5b**, in which four Cu^{I} ions cap to four alternate windows of the octahedral $\{Cu_6\}$ core. Color code: Cu^{II} ions and Cu^{II}-centered octahedra, cyan; Cu^{I} and Cu^{I}-centered trigonal pyramids, orange. (d) Axial elongation octahedron of the Cu1 cation: Cu1−O12 1.979(10), Cu1−O11 1.997(10), Cu1−N1 2.012(17), Cu1−N2 2.016(14), Cu1−O7B 2.408(10), and Cu1−O1C 3.006(10) Å. (e) 3D open-framework with **A**, **B**, and **C** channels along the *a*-axis in **5**. The C and H atoms, as well as water molecules are omitted for clarity. (f) Complex 3D intersecting channels in **5**. Color code: Cchannels **A**, cyan; channels **B**, blue; channels **C**, red. (g−i) View of three types of channels marked **A**, **B**, and **C** in the structure of **5**. The **5b** cluster unit not only fills in the channel **A** but also is located the cage surrounded by eight adjacent **5a** SBUs (g, channel A); the C atoms of the enMe ligands point into the inner of the channel **B** (h, channel B); whereas the lattice water molecules are filled in the channel **C** (i, channel C). (j) α-Po net topological net of **5** if each **5a** acts as a 6-connected node. (k) H-bonding interactions between **5b** and four **5a** SBUs. The N···O distance is 3.081 Å, and the O···O distances ranges from 2.597 to 2.979 Å. (l) Left /right helices in **5** along the [111] direction. The symmetry codes: B $2-y, 2-z, x$; C $-0.5-y, 1.5-x, 1.5-z$.

$M_6O_{19}^{8-}$ (M = V/Nb/Ta) and $M_6O_{19}^{2-}$ (M = Mo/ W) anions in POM chemistry. Thus, **5b** can be viewed as that four Cu^{I} ions cap to four alternate windows of the Lindqvist-type $\{Cu_6\}$ core through 12 μ_3−OH bridges. Such capping fashion was only observed in inorganic−organic hybrids $[(MCp^*)_4V_6O_{19}]$ (M = Rh/Ir),[18] so **5b** represents the first example of purely inorganic TM POM analogue.

Generally, POMs easily form discrete metal-oxo clusters with stable structure, but other TM ions cannot form purely inorganic TM-oxo clusters. Here, two different types of polynuclear TM complexes, $\{\mathbf{Cu_6}(enMe)_3(H_2O)_3\}$ and $\{Cu^{I}_4Cu^{II}_6(\mu_6\text{-}O)(OH)_{18}\}$ clusters in **5**, may be stabilized by trivacant POMs acting as mutidentate ligands and filling cavities in POM frameworks, where they form hydrogen bonds to neighboring TMSP units, respectively.

The bond valence sum (BVS) calculations[19] allow is to determine the oxidation states of the Cu centers and the location of the OH groups. The BVS values of the Cu3 and Cu4 ions are 2.09 and 1.08, indicating the oxidation states of +2 and +1, respectively. As to the O atoms except for the μ_6-O atom in **5b** cluster, the BVS values range from 0.51−1.16, suggesting these O atoms are monoprotonated. The oxidation states of the Cu centers are also in good agreement with their coordination geometries (octahedron and trigonal pyramid for the Cu3 and Cu4, respectively). The Cu^{I} ions result from the reduction of the Cu^{II} ions in the presence of the organic amine. It is a common phenomenon that the high oxidation state metals

(18) (a) Hayashi, Y.; , Ozawa, Y.; , Isobe, K.; , *Inorg. Chem.* **1991**, *30*, 1025, and references therein.

(19) (a) Brese, N. E.; O'Keeffe, M. *Acta Crystallogr., Sect. B* **1991**, *47*, 192. (b) Brown, I. D.; Altermatt, D. *Acta Crystallogr., Sect. B* **1985**, *41*, 244. (c) Thorp, H. H. *Inorg. Chem.* **1992**, *31*, 1585.

are reduced by organic N-ligands under hydrothermal conditions.[20]

Because of the high-symmetry cubic space group $P\bar{4}3n$, three types of channels in **5** are the same and intersect with each other in the perpendicular mode along the [100], [010], and [001] directions respectively, forming a 3D intersecting channels system containing two kinds of intersection: (a) three mutually perpendicular A channels intersect and (b) mutually perpendicular A, B, and C channels intersect, respectively (Figure 6f). Three types of channels can directly or indirectly communicate each other. Also, the well-regulated alignments of **5a** along the 3_1 screw axis generate the left/right helices along the [111] direction (Figure 6L). So far, such helices built by TMSP SBUs are rare in POM chemistry.[4c,7a]

Magnetic Properties. The magnetic behaviors of **2**−**5** are studied in the range of 2 to 300 K and the plots of χ_M, $\chi_M T$ versus T are shown in Figures 7 and 8. To quantitatively analyze the magnetic exchange interactions within hexa-Cu^{II} clusters in **2** and **4**, we applied the magnetic data of **2** and **4** to a theoretical model (inset of Figure 7a). At 300 K, the $\chi_M T$ value is equal to 2.73 emu mol^{-1} K for **2** and 2.38 emu mol^{-1} K for **4**, in approximate agreement with the expected value for six uncoupled Cu^{II} centers ($\chi_M T = 2.60$ emu mol^{-1} K assuming $g = 2.15$). Upon the compound being cooled from 300 to 75 K, the $\chi_M T$ value shows an approximate constant with a slight decrease. Below 75 K, the $\chi_M T$ value decreases rapidly as lowering temperature reaching the minimum of 0.78 emu mol^{-1} K for **2** and 0.46 emu mol^{-1} K for **4** at 2 K. The Curie−Weiss expression fits the magnetic susceptibility data of **2** between 2 and 300 K and **4** between 15 and 300 K affording Curie constant C = 2.82 emu mol^{-1} K and Weiss constant $\theta = -5.40$ K for**2** (see Figure S7 in the Supporting Information) and $C = 2.54$ emu mol^{-1} K and $\theta = -12.45$ K for **4** (see Figure S8 in the Supporting Information). The appropriate Hamiltonian for the hexa-Cu^{II} clusters in **2** and **4** can be written as Equation 1 with $S_1 = S_2 = S_3 = S_4 = S_5 = S_6 = 1/2$, regardless of the second- and third-neighbor interactions between Cu^{II} centers

$$H = -2J_1(S_1S_4+S_1S_5+S_2S_5+S_2S_6+S_3S_4+S_3S_6) - 2J_2(S_4S_5+S_4S_6+S_5S_6) \quad (1)$$

The molar magnetic susceptibility (χ) of hexa-Cu^{II} clusters in **2** and **4** is described as eq 2[21]

$$\chi = (Ng^2\beta^2/3kT)\{\sum S_n{}^T(S_n{}^T+1)(2S_n{}^T+1) \exp[-E_n/kT]\}/\{\sum(2S_n{}^T+1)\exp[-E_n/kT]\} \quad (2)$$

The magnetic susceptibility data of **2** and **4** have been computed using the MAGPACK program developed by Borràs-Almenar et al.[22] The best-fitting parameters are

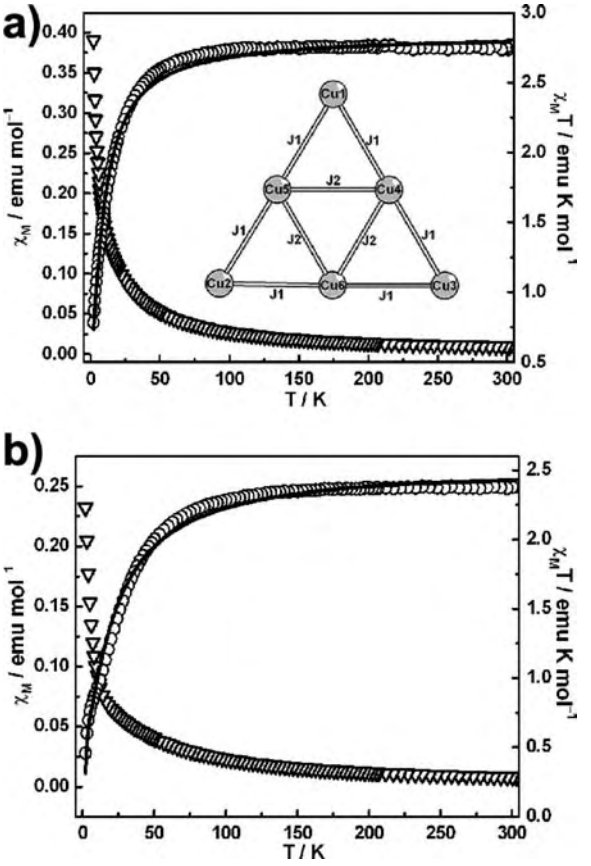

Figure 7. (a) Plots of χ_m and $\chi_m T$ vs T in the range of 2−300 K for **2**; (b) plots of χ_m and $\chi_m T$ vs T in the range of 2−300 K for **4**. The solid lines represent the best fit to experimental data.

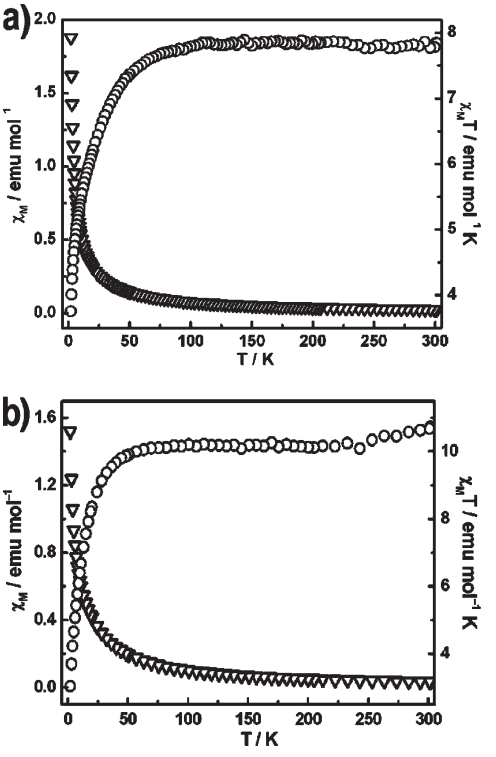

Figure 8. (a) Plots of χ_m and $\chi_m T$ vs T in the range of 2−300 K for **3**; (b) plots of χ_m and $\chi_m T$ vs T in the range of 2−300 K for **5**.

(20) (a) He, J.; Yin, Y.; Wu, T.; Li, D.; Huang, X. *Chem. Commun.* **2006**, 2845. (b) Cheng, J.-W.; Zheng, S.-T.; Ma, E.; Yang, G.-Y. *Inorg. Chem.* **2007**, *46*, 10534.

(21) Kahn O. *Molecular Magnetism*; VCH: New York, 1993.

(22) (a) Borrás-Almenar, J. J.; Clemente-Juan, J. M.; Coronado, E.; Tsukerblat, B. S. *Inorg. Chem.* **1999**, *38*, 6081. (b) Borrás-Almenar, J. J.; JClemente-Juan, M.; Coronado, E.; Tsukerblat, B. S. *J. Comput. Chem.* **2001**, *22*, 985.

$J_1 = -4.22\ cm^{-1}$, $J_2 = -4.86\ cm^{-1}$, $g = 2.26$, and $R = 2.0 \times 10^{-4}$ for **2** and $J_1 = -9.54\ cm^{-1}$, $J_2 = -11.45\ cm^{-1}$, $g = 2.13$, and $R = 6.4 \times 10^{-4}$ for **4** ($R = \Sigma[(\chi_M T)_{obs} - (\chi_M T)_{calc}]^2 / \Sigma[(\chi_M T)_{obs}]^2$). Additionally, a vast amount of research shows that the nature and strength of the exchange are chiefly affected by the Cu−O−Cu bond angles (Φ). The classical correlation between the experimental exchange constants and the Cu−O−Cu bond angles indicates that the complexes are generally antiferromagnetic for $\Phi > 98°$, whereas ferromagnetic for $\Phi < 98°$.[23] In **2** and **4**, the exchange pathway between each pair Cu^{II} ions are transmitted through one μ-oxo and one μ-O(H) bridge with Cu−O−Cu angles ranging from 90.2 to 108° for **2** and 89.9 to 105.8° for **4**, because more Cu−O−Cu bond angles are higher than 98°, the antiferromagnetic interactions are expected in these competitive environments.

For **3**, its magnetic behavior is very similar with those of **2** and **4** and indicates overall antiferromagnetic interactions among the Cu^{II} centers, which is also identified by the simulation of the Curie−Weiss law with $C = 7.96$ emu mol^{-1} K and $\theta = -3.75$ K (Figure S9). The $\chi_M T$ value shows an approximate constant with a slight decrease between 300 and 105 K, after 105 K, the $\chi_M T$ declines abruptly upon cooling and reaches the minimum of 3.76 emu mol^{-1} K at 2 K (Figure 8a). In fact, the antiferromagnetic interactions of the tetra-Cu^{II} $[Cu_4(H_2O)_2(\mathbf{PW_9})_2]^{10-}$ unit have been observed;[24] moreover, the structures of hexa-Cu^{II} $\{\mathbf{Cu_6PW_9}(en)_3(H_2O)_3\}$ units in **3** are also similar to those hexa-Cu^{II} units in **2** and **4**. Therefore, the hexa-Cu^{II} $\{\mathbf{Cu_6PW_9}(en)_3(H_2O)_3\}$ SBUs in **3** should exhibit antiferromagnetic interactions. Because the exchange interactions between the tetra-Cu^{II} $[Cu_4(H_2O)_2(\mathbf{PW_9})_2]^{10-}$ unit and two hexa-Cu^{II} $\{\mathbf{Cu_6PW_9}(en)_3(H_2O)_3\}$ SBUs can be ignored because of long Cu−O−W−O−Cu dis-tances, overall antiferromagnetic interactions in **3** are predictable in such a system.

For **5**, the value of χ_M slowly increases from 0.035 emu mol^{-1} at 300 K to 0.221 emu mol^{-1} at 45 K, and then exponentially to the maximum of 1.520 emu mol^{-1} at 2 K. At 300 K, the $\chi_M T$ value is equal to 10.73 emu mol^{-1} K, which is slightly lower than the spin-only value (12.40 emu mol^{-1} K) expected for thirty uncoupled Cu^{II} ions per formula assuming $g = 2.1$ (Figure 8b). Upon the compounds being cooled to 60 K, the $\chi_M T$ value shows a slight decrease. Below 60 K, the $\chi_M T$ value decreases rapidly with further cooling, reaching the minimum of 3.04 emu mol^{-1} K at 2 K. Such magnetic behavior is indicative of antiferromagnetic interactions within Cu^{II} centers. Fit the magnetic susceptibility data between 2 and 300 K to the Curie−Weiss expression affording Curie constant $C = 10.64$ emu mol^{-1} K and Weiss constant $\theta = -5.53$ K (see Figure S10 in the Supporting Information). The negative Weiss constant confirms the existence of antiferromagnetic interactions within Cu^{II} centers.

(23) (a) Ruiz, E.; Alemany, P.; Alvarez, S.; Cano, J. *J. Am. Chem. Soc.* **1997**, *119*, 1297. (b) Aromí, G.; Ribas, J.; Gamez, P.; Roubeau, O.; Kooijman, H.; Spek, A. L.; Teat, S.; MacLean, E.; Stoeckli-Evans, H.; Reedijk, J. *Chem.—Eur. J.* **2004**, *10*, 6476. (c) Shores, M. P.; Bartlett, B. M.; Nocera, D. G. *J. Am. Chem. Soc.* **2005**, *127*, 17986.

(24) Gomez-García, C. J.; Casañ-Pastor, N.; Coronado, E.; Baker, L. C. W.; Pourroy, G. *J. Appl. Phys.* **1990**, *67*, 5995.

Conclusion

In summary, a series of novel TMSPs from monomer, tetramer, 1D chain to 3D framework has been successfully made under hydrothermal conditions. The driving force of the assembly based on $\{\mathbf{Cu_6PW_9}L_3(H_2O)_n\}$ SBUs is mainly attributed to polyhedral distortion of the Cu^{II} ions, i.e. the Jahn−Teller effect of octahedra and pseudo-Jahn−Teller effect of square pyramids. Similar assembly has not been observed in TMSPs based on $\{\mathbf{Ni_6PW_9}L_3(H_2O)_n\}$ SBUs because no such effect exists in the Ni-polyhedra. The synergistic effect between five-coordinated poly hedra (trigonal bipyramid and square pyramid with pseudo-Jahn−Teller effect) and the octahedra with axial elongation (Jahn−Teller effect) reduces or overcomes the large steric hindrance, and benefits the occurrence of the assembly in **3** and **4**, respectively. For **5**, the Jahn−Teller effect of octahedra with axial elongation is considered as the driving force for the formation of **5**. Especially, the successful synthesis of **3** represents that different TMSP SBUs may combine and further construct novel larger aggregates under rational conditions, whereas the obtainments of **4** and **5** indicate that the same TMSP SBUs can self-polymerized to form extended frameworks. These interesting and meaningful findings encourage us to introduce other types of multivacant POM precursors (e.g., $[XW_{10}O_{36}]^{n-}$, X = Si/Ge/P; $[P_2W_{12}O_{48}]^{14-}$, and $[X_2W_{15}O_{56}]^{n-}$, X = P/As) into the ongoing system and further make novel poly(POM)s or open-frameworks drove by the Cu-based polyhedral distortion.

Acknowledgment. This work was supported by the National Natural Science Fund for Distinguished Young Scholars of China (20725101), the NNSF of China (50872133), the 973 Program (2006CB932904), the NSF of Fujian Province (E0510030), and the Knowledge Innovation Program of CAS (KJCX2.YW.H01).

Supporting Information Available: X-ray crystallographic files in CIF format for structures **1**−**5**; the IR spectra, PXRD patterns, TG curves, the plot of χ_m^{-1} vs T, and additional figures (PDF). This material is available free of charge via the Internet at http://pubs.acs.org.